UNIVERSITY OF CALIFORNIA, SAN DIEGO

Correlation Time of Ocean Ambient Noise Intensity in San Diego Bay and Target Recognition in Acoustic Daylight Images

A Thesis submitted in partial satisfaction of the requirements
for the degree Master of Science

in

Oceanography

by

Adam J Wadsworth

Committee in charge:

Professor Michael Buckingham, Chair
Professor Myrl Hendershott
Professor Jules Jaffe

2010

The Thesis of Adam J Wadsworth is approved, and it is acceptable in quality and form for publication on microfilm and electronically:

_____

_____

_____

Chair

University of California, San Diego

2010

DEDICATION

To the TSS.

EPIGRAPH

"...quel giorno più non vi leggemmo avante."

Nel mezzo del cammin di nostra vita
mi ritrovai per una selva oscura,
ché la diritta via era smarrita.

"Nessun maggior dolore
che ricordarsi del tempo felice
ne la miseria..."

E quindi uscimmo a riveder le stelle.

—Dante Alighieri

"I would prefer not to."

—Herman Melville

TABLE OF CONTENTS

LIST OF FIGURES

ACKNOWLEDGEMENTS

I wish to acknowledge Professor Michael Buckingham for his generous support and his guidance over the past year-and-a-half in his capacities both as my graduate adviser and as my thesis committee chair. In particular, I acknowledge Professor Buckingham's patience and understanding during a period of personal and health-related difficulties for me.

I wish to acknowledge each member of my thesis committee: Professors Mike Buckingham, Myrl Hendershott, and Jules Jaffe for their outstanding efforts as committee members over the past several months. I appreciate the valuable insight and feedback, both scientific and otherwise, that these gentlemen have provided me throughout the research process.

I also wish to acknowledge Chad Epifanio, whom I have never met but with whom I have shared much of the past year by way of his fifteen-year-old experimental data, code, and various writings. Indeed, Dr. Epifanio's doctoral work on acoustic daylight provided the inspiration for my own research into the subject.

Finally I wish to acknowledge my family, as well as the many wonderful individuals whom I am privileged to consider friends, for their tremendous support and frequent words of wisdom during my initial foray into graduate school.

ABSTRACT OF THE THESIS

Correlation Time of Ocean Ambient Noise Intensity in San Diego Bay and Target Recognition in Acoustic Daylight Images

by

Adam J Wadsworth

Master of Science in Oceanography

University of California, San Diego, 2010

Professor Michael Buckingham, Chair

A method for passively detecting and imaging underwater targets using ambient noise as the sole source of illumination (named acoustic daylight) was successfully implemented in the form of the Acoustic Daylight Ocean Noise Imaging System (ADONIS). In a series of imaging experiments conducted in San Diego Bay, where the dominant source of high-frequency ambient noise is snapping shrimp, a large quantity of ambient noise intensity data was collected with the ADONIS (Epifanio, 1997). In a subset of the experimental data sets, fluctuations of time-averaged ambient noise intensity exhibited a diurnal pattern consistent with the increase in frequency of shrimp snapping near dawn and dusk. The same subset of experimental data is revisited here and the correlation time is estimated

and analysed for sequences of ambient noise data several minutes in length, with the aim of detecting possible periodicities or other trends in the fluctuation of the shrimp-dominated ambient noise field. Using videos formed from sequences of acoustic daylight images along with other experimental information, candidate segments of static-configuration ADONIS raw ambient noise data were isolated. For each segment, the normalized intensity auto-correlation closely resembled the delta function, the auto-correlation of white noise. No intensity fluctuation patterns at timescales smaller than a few minutes were discernible, suggesting that the shrimp do not communicate, synchronise, or exhibit any periodicities in their snapping.

Also presented here is a ADONIS-specific target recognition algorithm based on principal component analysis, along with basic experimental results using a database of acoustic daylight images.

Chapter 1

ADONIS Ambient Noise Intensity Data

1.1 Description of the Data

Before performing any statistical analyses, a description of the ambient noise intensity data is required. Among the set of seventy-one storage compact discs are a number of files containing the raw data collected during the second set of ORB experiments in the autumn of 1995. Each data file contains a sequence of several thousand consecutive data frames representing several minutes (typically between ten and thirty minutes) of ambient noise intensity data recorded by the Acoustic Daylight Ocean Noise Imaging System (ADONIS) in San Diego Bay, Southern California [Epifanio et. al., 1999].

Each data file in the set consists of a file header structure followed by a sequence of frames, and each frame begins with its own short header structure. The file header contains important information about the data sequence under consideration, including: file size, date, time, data acquisition system (DAS) version, input channel, amplifier gain, and data packing method. Additionally, the file header often includes a character string containing a brief description of certain important qualitative and quantitative aspects of the experiment, for example: target type and location, environmental conditions, and scan and source details.

Relevant header information for each of the thirteen data files under consideration is recorded in Figure 1.1 and referred to throughout this document. Figure 1.2 describes the correspondence between data files in Figure 1.1 and the actual files stored on the 71 compact discs.

Each data frame contains the ambient noise information for one forty millisecond recording cycle, for each of sixteen frequency bins with centre frequencies spaced logarithmically between 8.5 kHz and 75.0 kHz, described in Figure 1.3. Each of the sixteen frequency bins is sampled separately and consecutively for about one millisecond each, with a gap of about 1.5 ms in between samples which allows for the signal to settle before sampling. The forty millisecond sampling cycle is repeated continuously for the entire length of the experiment so that the number of cycles is equal to the total number of data frames captured by ADONIS. Each of the 126 channels of the elliptical 11-by-14 ADONIS hydrophone array (shown in Figure 1.4) is sampled simultaneously for each of the sixteen frequency bins during each cycle [Epifanio, 1997]. Each frame, therefore, contains 2016 real-valued ambient noise intensities in units of amplitude in terms of analogue-to-digital (A/D) counts. These 2016 data points are typically reshaped at a later stage into a more spatially representative 16-by-126 data array. The data points are real-valued, as the imaginary part has been lost in a squaring operation during the data acquisition process.

1.2 Data Extraction and Processing

The thirteen files listed in Figure 1.1 were located among the 71 storage CDs by matching file date, time and other details. Initially, the first fifteen thousand frames (representing about ten minutes of acoustic noise data) along with the header information of each of the thirteen files were extracted, stored as in MATLAB variables, and then saved to a (as of 2010) forward-compatible MATLAB workspace file (in .mat format). Later, additional sequences of frames contained in select files were extracted in the same way, as necessary. This procedure was conducted using a now-obsolete version of MATLAB (4.2d), run on a Macintosh

machine (Mac OS X 10.2.4 (6J54), Power Mac G4 version 3.3, 2x512 MB RAM, 1.416 GHz, 167 MHz bus speed) in an emulated classic environment. This particular version of MATLAB was required in order to properly access the data files, which were unreadable with other versions of the program. The program-specific RAM had to be increased to the maximum 700000 kilobytes and the program restarted before each extraction to avoid running out of memory. Several unsuccessful attempts were made to extract the data with more recent versions of MATLAB using both PC (Windows and emulated Mac environments) and Mac machines before the correct and so far only workable environment-version pair able to handle the data file structure was found. It should also be noted that substantial time and effort were expended in the overall search for a workable method for extracting the ADONIS data from storage CDs, which significantly reduced the time available for other aspects of this project.

The data in each file was extracted twice: once to obtain a raw uncalibrated data sequence, and once to obtain logarithmic calibrated data sequence. In the first extraction, the data had its bad points removed and was linearized, but was kept non-equalized and uncalibrated, and ultimately left in terms of the raw ambient noise A/D count values. In the second extraction, the data was first linearized, then equalized and ultimately calibrated into intensities with units of (dB re 1 μPa^2/Hz). By convention, an extracted raw data file will contain raw in its file name, and the extracted data file linearized, equalized, and calibrated into intensities contain cal in its file name. These conventions are useful in quickly identifying the type of extraction in cases where the extracted data files name is explicitly stated.

The purpose of the linearization step is to limit the data values to below a certain threshold representing the divide between linear and nonlinear data. For calibrated data, this process ensures that no nonlinear data points are carried over to the equalization and calibration steps which are valid only for linear data. The nonlinear threshold is calculated based on header information (which in turn is generated during data acquisition). The data has global extrema in the A/D count range [0, 4095]. For data not being calibrated, the nonlinear threshold is still enforced as a kind of clipping operation, whereby only data within the range

[0, 4095] is considered valid. This range is evident in the raw ambient noise time series plots presented in Figure 1.5. In addition, in order to avoid $log(0)$ in the calibration step described below, all values of zero (dead elements, true values of zero, and others) are set to one. The final data range is therefore [1, 4095].

Equalization is performed by multiplying the data matrix by an equalization matrix. The equalized data reflects the true value of the bin voltage observed at the electronics output. The equalization data is stored as a matrix of constant values in linear units. The manner by which these values are computed is described by Epifanio [1997]. The voltage conversion and A/D gain values are incorporated into the equalization matrix and the equalization values are created from actual ambient noise data so that any channel variations due to reflector gain are corrected for automatically. The equalization matrix values have a one-to-one correspondence with the ADONIS hydrophone array channels.

The calibration is performed in log space on the equalized ambient noise data. Neglecting the reflector, ADONIS can be considered a type of multi-channel noise meter and so a modified noise meter calibration method is employed [Epifanio, 1997]. The calibration matrix, C, as well as the dish-gain-per-bin matrix, G, are subtracted from the scaled base-ten log of B, the equalized data (estimate of the RMS energy amplitude), to give the equivalent noise power spectrum level, or PSL:

$$PSL = 20log(B) - C - G, \tag{1.1}$$

where the PSL is in units of (dB re 1 μPa^2/Hz). This relationship is valid as long as B^2 is proportional to PSL, and as long as the amplitude of the input ambient noise is low enough to keep the ADONIS electronics within the linear operating region (consistent with the discussion on bad and nonlinear data earlier in this section). It is ultimately the PSL values for the top three frequency bins (bins 14 to 16, or equivalently 57 kHz to 75 kHz centre frequencies) that are used to form meaningful acoustic daylight images of an underwater target. This particular frequency range yields largest intensity difference ($3dB$ after calibration) between beams that intersect the target and beams that do not intersect the target.

Beam pattern analysis reveals that the beam width for a source at 25m from ADONIS ranges from 0.68 degrees at 75 kHz to 3.36 degrees at 10 kHz. It should be noted that the beam width progression with frequency is not smooth; the beam widths do not scale inversely with frequency [Epifanio, 1997]. Like the equalization matrix, the calibration (C) and dish-gain-per-bin (G) matrices are predetermined constants. These matrices are chosen based on the type of experiment and gain information found in the data file header, and are then loaded and applied to the data. The calibration and dish-gain-per-bin matrices are functions of all other relevant parameters in the noise meter calibration method, for example: element sensitivity, electronics and reflector gains, and equivalent solid angle for the beam.

In both extraction cases, the so-called bad frames were identified (and their locations recorded) and were removed during extraction. A good frame is one with a conversion pulse count of 2048 recorded in the frame header, while a bad frame is one for which a spurious memory transfer occurred during the data acquisition sequence, and is identified by a conversion pulse count of less than 2048. The bad frames are therefore unreliable as data points and should be omitted from any data analysis. The bad frames represent less than five percent of the frames in each file and seem to be randomly distributed. A consequence of omitting the bad frames is that the information contained in each bad forty millisecond interval will be lost and the corresponding time interval is reduced to zero. In addition, the entire time interval represented by the sequence of frames will be a few percent smaller than the actual time interval during which the data was recorded. The time distortion and the loss of information have the potential to change the auto-correlation estimation calculation (which is time dependent) and thus adversely affect the correlation time analysis. Similarly, the loss of information due to the removal of nonlinear data (described in the linearization step above) may also negatively affect the correlation time analysis.

1.3 Isolating Useful Data Segments

Initially considered for correlation time analysis were segments of at least fifteen thousand consecutive frames, representing at least the first ten minutes of each of the thirteen ADONIS ambient noise data files described in Figure 1.1. The minimum of ten minutes reflects both the length of time used by Epifanio [1997] in his statistical analysis as well as a practical size given the maximum RAM available in the old version (4.2d) of MATLAB used data extraction. Longer segments (up to the total length of the experiment) were occasionally used (in the case of data file number 15, for example), but were more difficult to obtain as they required a post-extraction matching of two or more separately extracted data segments. Only the raw ambient noise intensity data in units of A/D counts was used for the correlation time analysis, since data calibrated in log space into units of decibels is nonlinear and cannot produce a useful correlation time plot. For compactness and comparison purposes, the auto-correlation curves for raw data from several frequency bins were generally superimposed on a single plot.

To view the general behaviour of the intensity of the ambient noise over time, a simple time-series plot of raw ambient noise data counts over time (in seconds) was produced for each of the thirteen files listed in Figure 1.1. For illustration and completeness purposes, a time-series plot for a single data file, number fifteen, is shown in Figure 1.5, which may be considered typical in many respects of all thirteen files time series plots. The ambient noise intensity data from each of the sixteen frequency bins described in Figure 1.3 was examined; the intensity trend was found to be similar for any given frequency bin. Only the top four frequency bins, 13 through 16, are presented in Figure 1.5. All data presented in the figures was recorded by a single hydrophone, number 12, which is approximately at the centre of the hydrophone array. The numbered spatial configuration of the hydrophone array is shown in Figure 1.4. Time-series plots were generated using data from hydrophones at other locations (including, in particular: channels 26, 116, 90, and 73), and these turned out to be similar but not identical in overall shape. The existence of a readily detectable difference in noise intensity among hydrophones at different locations in the array is consistent with the intensity dif-

ferences (on the order of 3 dB) readily observed among pixels of the calibrated acoustic daylight images.

There are some features of note in the time-series in Figure 1.5. The ambient noise intensity upper limit of 4095 A/D counts is evident throughout the time-series, which is consistent with the linearisation step in the extraction restricting the raw data to the range [1, 4095]. The hard upper threshold does not appear to have affected a large percentage of the data points. Also, it is evident that there was a non-trivial minimum ambient noise intensity on the order of 10 A/D counts (with a typical range of 30 to 90 A/D counts) throughout the entire sequence indicating a continuous non-zero minimum background noise level. As the snapping shrimp were the single most significant high-intensity noise source, it is likely that the shrimp contributed at least in part to this continuous minimum background noise level.

The most significant feature evident in Figure 1.5 is the prominent spike in minimum (and overall) noise intensity centered at approximately 620 seconds coincides with the ADONIS hydrophone array being rotated (or scanned) horizontally across the target. The data file header indicated there was a scan from left to right across the target at some point during the experiment. Each of the first 18951 good data frames, equalized and calibrated into intensities in dB during extraction, was transformed into an individual acoustic daylight image by averaging the top three frequency bins (57kHz to 75kHz). The sequence of 18951 images was then made into an acoustic daylight video and the left to right scan across the target was confirmed visually between (approximately) the 600 and 630 second marks. This process was repeated for the other twelve data files as a means of locating and confirming ADONIS scans across a target and other visually detectable events.

It can also be seen in Figure 1.5 that that the upper limit of 4095 A/D counts affected only a small percentage of the data points during the first ten minutes of data where the ADONIS is in a static configuration (that is, not scanning). However, this hard threshold became quite significant when the ADONIS scanned horizontally across the target. It is evident in the time series (and in particular for frequency bins 13 through 16) that for several seconds during the scan represented

by the intensity peak, every data point was cut off and assigned a value of 4095 A/D counts. In the video, this event was represented by a near-still image for these several seconds, trivially displaying the constant intensity values represented by the calibration and equalization matrices. The most likely explanation for this abrupt departure from the static configuration is that the loud hydraulic device driving the rotation of ADONIS temporarily overwhelmed the entire ambient noise field. The acoustic image became completely saturated for several seconds during the scan and the target was no longer visible during that time. This phenomenon was not always so severe; in most of the experiments the scans resulted in a much smaller jump in intensity and only rarely was there a significant period of time where the intensity was continuously cut off for several seconds at the 4095 A/D count limit.

#	Name (Table)	Name (Parms: Desc)	Total Length (min)	Sample Length (min)	Start Time (Table)	Start Time (Parms)	Sun Rise/Set (timeand... date.com)	Date	Day	Tide	Traffic	Wind	Target Dist	Scan Detail	Source	Source on When?	A/D board Gain
2	MM2(1)	Multimetal2	~22	~10	7:10:00	7:20:03	6:07:00	11/2/1995	Th	high	low	no	40m	L, R			8
3	HoleyC	HoleyCross	~21	~10	8:35:00	8:35:41	6:10:00	11/6/1995	M	high	low	no	40m	L, R			8
4	MMscan	Multi-metal targets	~17	~10	9:10:00	9:11:04	7:01:00	10/26/199	Th	rising				back & forth across target			8
5	Wood	Multiwood	~25	~10	11:24:00	11:24:56	6:08:00	11/3/1995	F	falling				L,R	45kHz, 0.03 Vpp; suspended from buoy to left of frame	first & last minute	8
7	Xscan	Foam Drum?	~21	~10	12:32:00	12:33:22	7:00:00	10/25/199	W	falling	lots of boats	picking up		L till foam drum, the R till dolphin pens, then back to target frame			8
8	Sphere	Titanium Sphere	~26	~10	14:30:00	14:30:44	16:54:00	11/6/1995	M	low			~45m	L, R	45kHz, 0.03 Vpp	first & last minute	1
9	SandAir	2 drums from homemade platform (2x4); sand(L), air (R), sep=12ft	~32	~10	15:24:00	15:24:13	18:03:00	10/27/199	F	falling			~45m	across	45kHz, 0.25 Vpp	during first scan to left	8
10	FarPlus	"+"	~10	~10	16:25:00	16:25:11	17:00:00	10/30/199	M	falling			80m	L, R			8
11	FarX	X	~12	~10	17:06:00	17:06:02	16:59:00	10/31/199	Tu	falling	low		80m	panning L, R; starting at ~339			8
13	FarC	Holey-cross	~27	~10	17:45:00	17:45:43	17:00:00	10/30/199	M	falling	low	calm	80m	L, R @ 1000psi			8
14	NearD	Three drums; air(L), water(C), sand(R)	~18	~10	17:56:00	17:56:50	16:56:00	11/3/1995	F	high			~20m	L, R			8
15	MM2(2)	Multimetal set 2; targets: 1/8" aluminum & no foam(L), 1/4" aluminum(C), corregated aluminum(R)	~25	~10	19:48:00	19:47:59	16:58:00	11/1/1995	W	falling			40m	L, R			8
16	3Drum	Drum trials: air(L), water(C), sand(R)	~20	~10	21:40:00	21:40:08	16:57:00	11/2/1995	Th	falling				on water drum, then L, R @ 1100psi	45kHz, 0.05 Vpp; on water drum	first minute ?	8

Figure 1.1: Subset of ADONIS ambient noise data files chosen for statistical analyses. Descriptive details obtained from Epifanio's doctoral dissertation [1997], as well as from data file header information. The numbers in the leftmost column correspond to the numbering in Table 8.1 of the dissertation.

Table 8.1 Number	Filename in Table 8.1	Storage CD Number (out of 71)	Filename on Storage CD
2	MM2(1)	65	MULTIMET.DAT
3	HoleyC	22	HOLEYCROSS.DAT
4	MMscan	37	MULTIMET.DAT
5	Wood	13	MULTIWOO.DAT
7	Xscan	7	XSCAN_1.DAT
8	Sphere	26	FARSPHER.DAT
9	SandAir	42	SANDAIR1.DAT
10	FarPlus	47	FARPLUS6.DAT
11	FarX	53	FARX_3.DAT
13	FarC	48	FARCRUC1.DAT
14	NearD	17	NEARDRUM.DAT
15	MM2(2)	62	MULTIME6.DAT
16	3Drum	67	3DRUM-3.DAT

Figure 1.2: Chart showing the experimental correspondence between the data files listed in Figure 1.1 and the data files among the 71 storage CDs.

Frequency Bin	Centre Frequency (kHz)
1	8.5
2	10.0
3	11.7
4	13.8
5	16.0
6	18.6
7	21.3
8	24.6
9	28.3
10	32.6
11	37.5
12	43.1
13	49.5
14	57
15	64.4
16	75.0

Figure 1.3: Centre frequencies, corresponding to each of 16 logarithmically spaced frequency bins, at which the intensity of the noise is sampled in each channel at 25 times per second (or approximately 4 ms per frame). This table is equivalent to TABLE I in [Epifanio et al., 1999].

				24	25	**26**	40	41	42				
		17	16	82	81	80	45	44	43	105	104		
	18	19	20	83	84	85	46	47	107	106	102	103	
79	78	23	22	21	87	86	48	49	108	109	101	100	99
74	75	76	77	15	14	13	51	50	111	110	119	118	117
73	72	8	9	10	11	**12**	52	53	112	113	114	115	**116**
5	6	7	71	70	69	68	55	54	120	59	58	57	56
4	3	2	64	65	66	67	123	122	121	60	61	62	63
	0	1	31	30	94	95	124	125	38	39	97	98	
		27	28	29*	93	92	91	37	36	35	96		
				88	89	**90**	32	33	34				

Figure 1.4: Spatial configuration of the receive-only hydrophones in the ADONIS hydrophone array. The numbers listed correspond to the original channel or multiplexer number associated with each hydrophone in the array. The ordering does not account for reversal of image (horizontal flipping) due to the dish. Channel 29(*) is dead in the ORB 2 experiments [Epifanio, 1997]. Select channels described in the statistical investigations are: 12 (center-mid), 26 (top-mid), 90 (bottom-mid), 116 (center-right), and 73 (center-left).

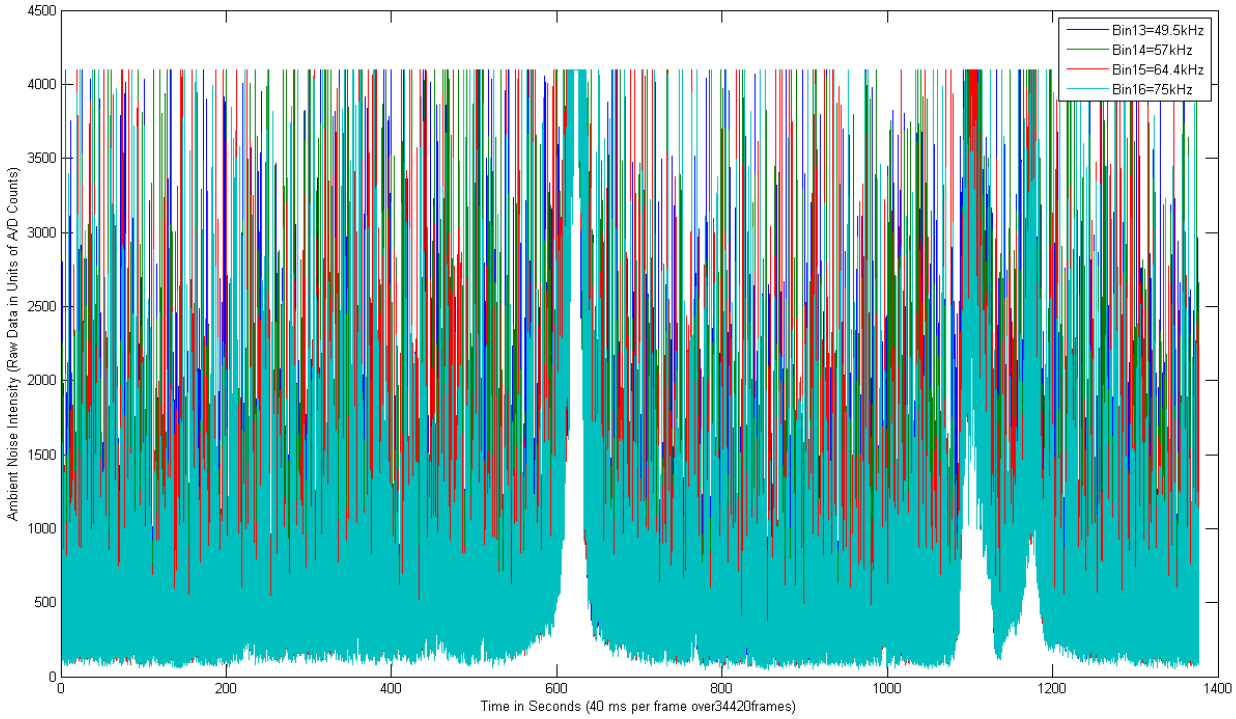

Figure 1.5: Ambient noise intensity time series for data file number 15 (described in Figure 1.1). The intensity units are in A/D counts. The 34420-frame sequence represents the raw experimental data in its entirety. The spikes in minimum intensity (e.g. near 600 seconds and 1100 seconds) represent times where the ADONIS is scanning horizontally over the target. At other times, where minimum intensity remains relatively constant, the ADONIS is motionless; a static configuration. A subset of the frequency bins (13 through 16) are shown here.

Chapter 2

Correlation Time Analysis of Ambient Noise Intensity

2.1 Auto-correlation Algorithm

In the correlation time analysis for the ADONIS ambient noise fluctuations, the desired time correlation function is the special case of the cross-correlation: the auto-correlation, in which the two input sequences being considered are the same. In this case, the quantity being considered is a sequence of raw ambient noise intensity data over time. The purpose of the auto-correlation in this case is to quantify the similarity between noise observations in a single data set as a function of the time separation (or time lag) between them. According to Buckingham [1983], a continuous, time-dependent, random process represented by the real function $x(t)$, has a true auto-correlation:

$$R_{xx}(\tau) = \lim_{T\to\infty} \int_{-T/2}^{T/2} x(t+\tau)x(t)dt, \tag{2.1}$$

where t represents time, $\tau = s - t$ represents a time lag or time separation between two times, t and s, where t and s may be different or equal. $R_{xx}(\tau)$ is therefore the auto-correlation between the process x at time t and the same process x at time s. The auto-correlation at zero time, $R_{xx}(0)$, will be the location of the biggest peak, and is equal to the mean-square value of the process $x(t)$. This is expected since

two signals which are the same will be exactly correlated at the same time lag. At no time lag are two identical signals better correlated than at $\tau = 0$. A normalized auto-correlation, where the auto-correlation at zero lag is identically one, will have the maximum value of one at the origin. If $x(t)$ contains a periodic component, the (true) auto-correlation will also contain a periodic component with the same period. However, if $x(t)$ does not contain a periodic component, the (true) auto-correlation will tend to zero as the time lag goes to infinity, that is, $x(t+\tau)$ becomes increasingly uncorrelated with $x(t)$ as the lag τ becomes larger. Also, the auto-correlation of a real function is an even function, so one can expect a plot of the auto-correlation function to be symmetric about the origin, $t = 0$, as is the case with the analysis here.

Since any given ADONIS ambient noise data sequence (which is several minutes in length) is a discrete, finite segment of one realisation of the theoretically infinite-length process represented by the ocean's ambient noise field, the correlation time for the ambient noise intensity cannot be calculated using the real auto-correlation described in 2.1. Instead, it must be estimated using a deterministic auto-correlation algorithm based on the true auto-correlation. The algorithm used here is an efficient FFT-based cross-correlation algorithm that can handle auto-correlation as a special case [Orfanidis, 1996], implemented as xcorr in the standard MATLAB signal processing package. For a discrete real process $x(t)$ of time-length T defined as $x(0), x(1), ..., x(T)$, where each element is a sample of the process $x(t)$, the raw, discrete, non-normalized auto-correlation estimate is computed for non-negative time lags τ in the following way:

$$R_{xx}(\tau) = \sum_{t=0}^{T-\tau-1} x(t+\tau)x(t). \tag{2.2}$$

By the basic properties of the auto-correlation for the real process $x(t)$, the auto-correlation curve over time will be symmetric about $t = 0$, so $R_{xx}(\tau) = R_{xx}(-\tau)$ for all time lags. Given the special case where both input sequences are the process $x(t)$ of length T, the cross-correlation algorithm returns an output sequence of values of length $(2T-1)$ representing the corresponding auto-correlation sequence estimate. The calculation involves an implementation of 2.1. The output sequence

is $c(\tau) = R_{xx}(\tau - T)$, where $\tau = 1, ..., (2T - 1)$. The normalization scheme used here for the auto-correlation is one where a normalization constant is calculated based on the constant coefficients of the raw auto-correlation sequence values, and each value in the sequence is divided by that normalization constant so that the auto-correlations at zero lag ($\tau = t = 0$) are identically unity (represented by a steep spike about zero lag).

2.2 Auto-correlation of White Noise

As a consistency check and for the purpose of future comparison with ambient noise correlation time plots, a short experiment was undertaken involving synthetic data and their auto-correlations. Four sequences of five hundred pseudo-random numbers were generated using the Ziggurat algorithm [Marsaglia and Tsang, 2000]. The first two sequences were formed from a uniform distribution in $[0, 1]$ and then multiplied by a constant ($a = 2000$) after being centered about either $f(t) = 0.5$ (the regular configuration) shown in blue, or shifted by a constant value of 0.5 (so as to be centered about $f(t) = 0$) shown in red. The second two sequences were formed from a normal distribution with mean 0 and standard deviation 1 that was multiplied by a constant ($a = 2000$) after being centered about either the origin (a mean of 0), shown in black, or one (a mean of greater than 0), shown in green. These four curves are superimposed in Figure 2.1. Subsequently, the auto-correlations of the random functions plotted in Figure 2.1 were plotted and are presented in Figure 2.2.

It is evident that those sequences originally centered at a point above the origin (that is, with a mean greater than zero) exhibited a distinct triangular windowing effect. This windowing effect is characteristic of the auto-correlation of a (finite) square pulse of positive constant value. The auto-correlations of the green and blue curves of Figure 2.1 clearly exhibited such a triangular windowing effect. The curves representing these auto-correlations are illustrated using the same colour scheme in Figure 2.2. Meanwhile, those functions that were centered about the origin (that is, with a mean of zero) exhibited no such triangular

windowing effect. Moreover, they approximated the delta function that would be expected of the auto-correlation of finite white noise. The curves representing these auto-correlations are the red and black curves of Figure 2.2.

A basic conclusion drawn from this experiment is that subtracting the mean from each point in the original time-series, so that the time-series is centered about the horizontal origin, allows for the generation of an auto-correlation plot devoid of any triangular windowing artifact. This allows the other features of the correlation time to be more readily observed by inspection. Of particular interest in the eventual correlation time analysis of the ambient noise data is the behaviour of the curve near the origin (lag of zero), where the de-correlation is fastest. This region can be better examined once the windowing artifact is removed.

2.3 Auto-correlation of Ambient Noise Intensity Data

A correlation time analysis of ADONIS data file number fifteen of Figure 1.1 is examined in detail in this section, and is representative of the procedure used for the analysis of the remaining thirteen experimental data files. The entire 34420-frame ambient noise intensity sequence, whose original time-series plot is presented in Figure 1.5, is again considered here. It is evident that the 34420-frame sequence contains both sub-sequences where the ADONIS is in a static configuration (that is, motionless), and sub-sequences where the ADONIS is scanning horizontally across the target (that is, in motion). By way of acoustic daylight image video, the non-static configuration sub-segments were verified as coinciding with the large spikes in minimum intensity in the time-series plots, and the static configuration sub-segments were those sections with relatively constant minimum intensity in the time-series plots. It is important to note that the ADONIS scanning operation was powered by a noisy hydraulic motor [Epifanio, 1997], which almost certainly accounts for the aforementioned large intensity spikes (and departure from the typical minimum ambient noise level of $O(10)$ A/D counts).

The normalized auto-correlation algorithm developed in Section 2.1 and

applied to random data in Section 2.2 was applied to data file fifteen by way of using the entire 34420-frame ambient noise intensity sequence as the input sequence. A relevant subset of frequency bins was considered: three of the lower frequencies (bins 1, 5, and 9), as well as the top four frequency bins (13 through 16) which are also those four frequencies depicted in Figure 1.5. Plots of the resultant auto-correlations over time are presented in Figure 2.3. Of particular note in the auto-correlation curves are the general triangular shapes of the curves and their resemblance to the triangular windowing artifact depicted in the blue and green curves in Figure 2.2. Also of note are the spikes in auto-correlation near 600 seconds and 1200 seconds, which roughly correspond to the temporal locations of the spikes in ambient noise intensity (around scanning episodes) in the time series plot in Figure 1.5. Finally, it is evident that the shape of the auto-correlation curve in first minute around $t = 0$ deviates quite distinctly from a typical delta function approximation, and looks to exhibit behaviour possibly approximating an exponential decay. However, since it is known by way of ADONIS data file header information as well as visually in the acoustic daylight video that segments of data were contaminated by sharp bursts of the hydraulic motors high-intensity noise, it is likely that the auto-correlation estimations for the time lags around $t = 0$ were significantly affected by the non-static configuration scanning events. It is therefore imperative to compare the result described previously in this paragraph with the auto-correlation results for static configuration segments only. Such a segment is obtained using the method described in Section 1.3 (Isolating Useful Data Segments).

The normalized auto-correlation curves over time of the initial 560 seconds of ambient noise intensity contained in data file number 15 are presented in Figure 2.4. This 560 second segment was verified by acoustic daylight image video to correspond to a period of time where the ADONIS is in a static configuration, that is, not scanning horizontally across the target. The same representative subset of the frequency bins (described in the previous paragraph) is considered. The original time series is just the first 560 seconds of the time series plotted in Figure 1.5. Again note the triangular shapes of the curves and their resemblance

to the triangular windowing artifact depicted in the blue and green curves in Figure 2.2. This will be dealt with in the next paragraph. Note also the absence of any spikes in auto-correlation evident in Figure 2.3. This almost certainly reflects the absence of any scanning events during this 560 second segment, so the data is largely representative of the ambient noise field in San Diego bay at the time, which in turn is largely dominated by the shrimp snapping activity. Finally, note the approximate delta-function shape of the auto-correlation curve near $t = 0$. The possibly exponential-looking behaviour near $t = 0$ is completely absent, and the normalized auto-correlation curves drop by about fifty percent after the first forty millisecond time lag, that is, just one data frame period. This confirms the result predicted in the previous paragraph.

Figure 2.4 presents the normalized auto-correlations of the mean-biased initial 560 seconds of ambient noise intensity time series of data file number 15. The mean bias is applied by subtracting overall mean value (531.84 A/D counts) from each data point in each time series prior to auto-correlation. Figure 2.4 is therefore the same as Figure 2.3 except for the mean-biased time-series input. Note the approximate delta-function shape of entire auto-correlation curve in the absence of any triangular windowing artifact. The removal of the mean before auto-correlation is effective in eliminating the triangular windowing in the same manner as for the random data presented in Figure 2.1 and Figure 2.2, and comparing those two auto-correlation curves with the curve in Figure 2.4, it is clear that the auto-correlation of a segment of static-configuration ADONIS ambient noise intensity data closely resembles the zero-mean auto-correlation curves for white noise (red and black) presented in Figure 2.2. It is reasonable to assume, therefore, that the shrimp-snap-dominated ambient noise intensity fluctuations in San Diego bay are simply white noise and exhibit no periodicities at timescales smaller than the diurnal intensity increases around dusk and dawn demonstrated by Epifanio [1997]. A basic conclusion that may be drawn from these results is that since the shrimp seem to not exhibit any kind of synchronization or pattern that might manifest itself as a periodic or other non-white-noise signal (which would appear as something other than a delta function upon auto-correlation) it is very likely

that the shrimp do not co-ordinate or communicate by snapping, or otherwise care about each others' snaps.

To help confirm the results, a horizontally-constrained zoom of Figure 2.5 is presented in Figure 2.6, which more clearly illustrates the behaviour of the auto-correlation curve near $t = 0$. Note the extremely rapid de-correlation of the ambient noise intensity over the a 0.04 second (or one frame) time lag. It is again evident that the auto-correlation of the ambient noise intensity in the initial mean-biased static-configuration segment of ADONIS data file number 15 very closely resembles a finite approximate to the delta function, the auto-correlation of white noise, which is equivalent to the auto-correlation curve for a random sequence of numbers with a mean of zero described earlier in this section. This result is common to several sections of ambient data from different files (representing experiments on different days and at different times for different targets). The result also holds for all 16 frequency bins (between 8.5 kHz and 75.0 kHz), and for hydrophones at various locations in the array.

Some concerns exist about the validity of the results. First, it is possible that the raw noise intensity data is not truly representative of shrimp snaps as the dominant high-frequency ambient noise source, and instead is heavily contaminated by white noise from the amplifier assemblies, the electronics, the hydraulic scanning motor, and other sources (apparatus and environmental) not accounted for in the subjective description of the experimental site. This is unlikely as the hydraulic motor effect is removed by isolating only static-configuration data, and the other noise sources have been very carefully analysed and checked by Epifanio over the course of his doctoral work [1997]. Second, the application of a hard threshold to the raw ambient noise intensity of 4095 A/D counts (the upper limit for linear data) may remove too much information and hide some potential periodicities at the highest intensity levels. Similarly, throwing away both nonlinear and bad frames during extraction (which represent 5 percent of the total) may remove too much information, introduce unacceptable data gaps, and otherwise render the auto-correlation estimation calculation invalid by adulterating or distorting the continuity of the time lag intervals. Since the bad frames seem to be randomly

distributed throughout the data and represent such a small percentage of the data, it is assumed here that the result of an auto-correlation representing white noise would not be affected by reintroducing any of the removed data. Third, the small noise recording time window afforded to each frequency bin (about 1ms out of each 40ms recording cycle) may cause some aliasing or otherwise result in an unacceptable loss of information. This is a valid concern, and might be addressed by some more creative averaging or other pre-processing of the data prior to auto-correlation, but the concern is mitigated somewhat in that the time-series curves and auto-correlation curves for each frequency bin exhibit very similar behaviour in each case, so any missed periodicities, for example, would need to be extremely well-hidden in order to be concealed by the sampling process in the ADONIS experiments.

Future data analysis on this same data set may help address some of the issues addressed in the previous paragraph, and also help confirm the results outlined earlier. Figure 1.1 outlines the various experimental variables that have the potential to significantly affect the time-series as well as correlation time behaviour of the ambient noise field in San Diego Bay. Some such significant variables might include: target shape, size, material distance from ADONIS, angular direction from ADONIS, distance from sea floor; time of day (especially with respect to the known diurnal variations in shrimp snapping), length of experiment, day of the week; noise intensity, frequency and directionality of boat traffic and industrial noise, marine mammal vocalizations (which have a directional dependence, e.g. marine mammal pens at 180 degrees), and other potential significant noise sources other than the known dominant shrimp snapping; tide behaviour and effects; wind, air and water temperature, precipitation, and other weather effects; ADONIS scanning details including direction, duration and speed, depth; A/D board gain (note file number 8 in Figure 1.1 has an A/D board gain of 1 instead of the usual 8); the effect of occasional explicit introduction of a known-frequency experimental noise source and its characteristics; experimental synchronization with the camera and ITC; and differences between data recorded spatially disparate array hydrophones. Many of these variables have already implicitly been ruled out

(through careful consideration in Epifanios [1997] as well as my own analysis) as being able to significantly mask or distort the outcome of the experiment based on the assumption of the shrimp snapping as the dominant ambient noise source in San Diego Bay, but it certainly would not hurt to have additional objective analysis in order to confirm the results present in this document.

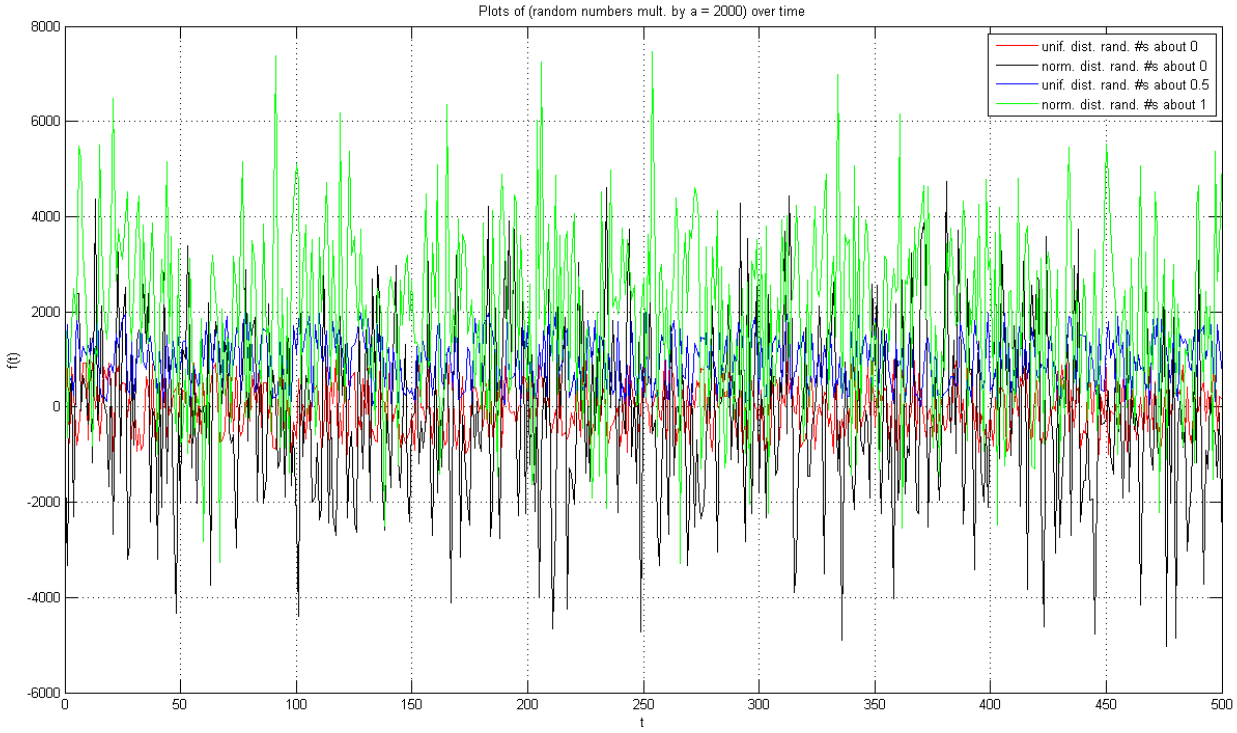

Figure 2.1: Superimposed plots of sequences of 500 pseudo-random numbers generated using: (a) uniform distribution in $[0, 1]$ (red/blue), and (b) normal distribution with mean 0 and standard deviation 1 (black/green). The first two plots (red/black) are shifted (if necessary) so as to be centered about the origin (i.e. mean $= 0$), and the second two plots (blue/green) are shifted (if necessary) so as to be centered above the origin (i.e. mean > 0). Note that all random values have been multiplied by a constant ($a = 2000$) after having been generated using the parameters above.

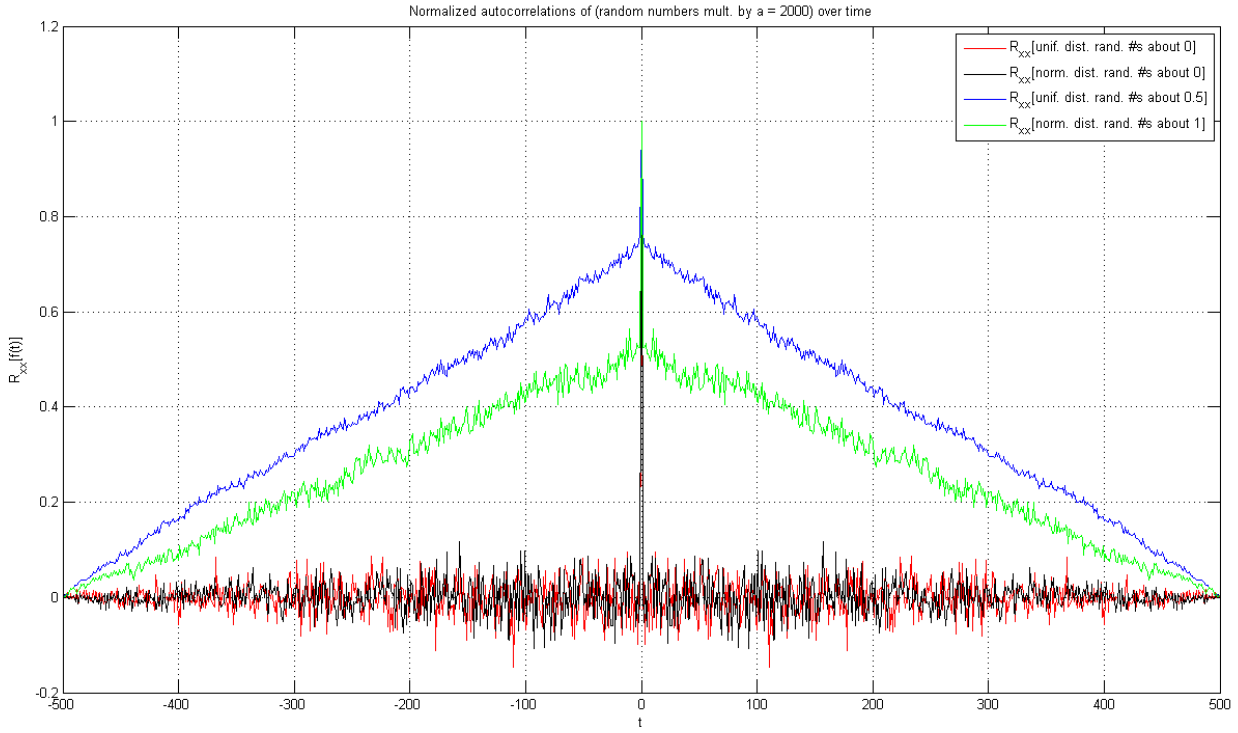

Figure 2.2: Normalized auto-correlations of the random functions plotted in Figure 2.1. Note that those functions (blue/green) that were centered above the origin (i.e. mean > 0) exhibit the same triangular windowing effect as the unbiased (i.e. not shifted by the mean) ADONIS ambient noise intensity auto-correlation plots elsewhere in this chapter. Those random functions that were centered about the origin (i.e. mean $= 0$) exhibit no such triangular windowing effect, and approximate the delta function which is the expected auto-correlation of finite white noise.

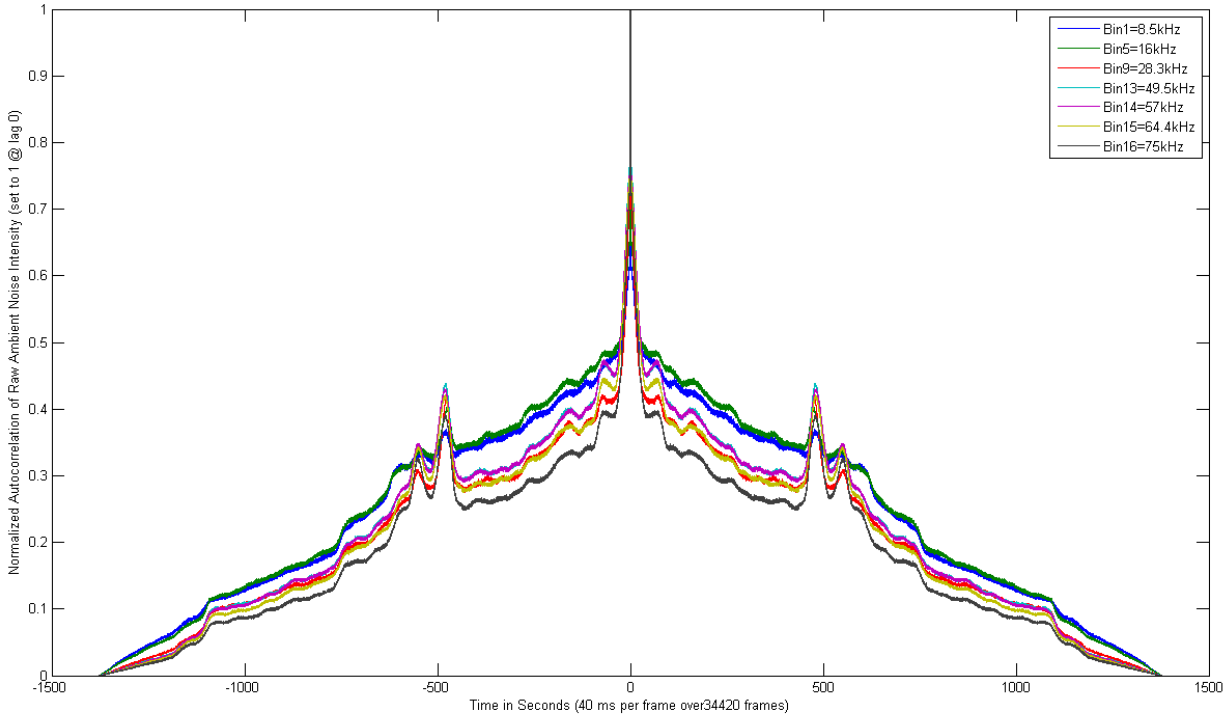

Figure 2.3: Normalized auto-correlations of the ambient noise intensity time series of data file number 15. A representative subset of the frequency bins is considered. The original time series were plotted in Figure 1.5. Both static configuration (motionless ADONIS) and non-static configuration (ADONIS scanning across the target) segments are present. Note the triangular shapes of the curves and their resemblance to the triangular windowing artifact depicted in the blue and green curves in Figure 2.2. Also note the spikes in auto-correlation near 600 seconds and 1200 seconds, which roughly correspond to the temporal locations of the spikes in ambient noise intensity (around scanning episodes) in the time series plot in Figure 1.5. Finally, note shape of the auto-correlation curve in first minute after $t = 0$ and its deviation from a typical delta function approximation.

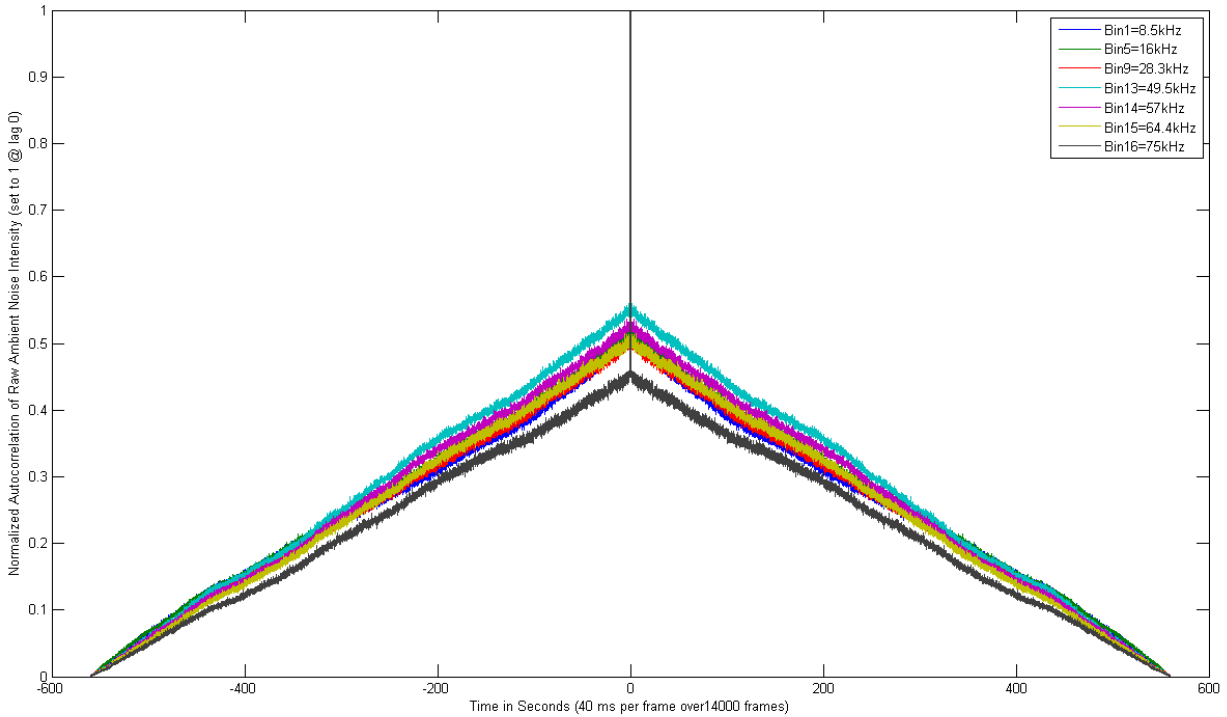

Figure 2.4: Normalized auto-correlations of the initial 560 seconds of ambient noise intensity time series of data file number 15. This 560 second segment was verified by acoustic daylight image video to correspond to a period of time where the ADONIS is in a static configuration, that is, not scanning horizontally across the target. A representative subset of the frequency bins is considered. The original time series is the first 560 seconds of the time series plotted in Figure 1.5. Again note the triangular shapes of the curves and their resemblance to the triangular windowing artifact depicted in the blue and green curves in Figure 2.2. Note the absence of any spikes in auto-correlation evident in Figure 2.3. Finally, note the approximate delta-function shape of the auto-correlation curve near $t = 0$.

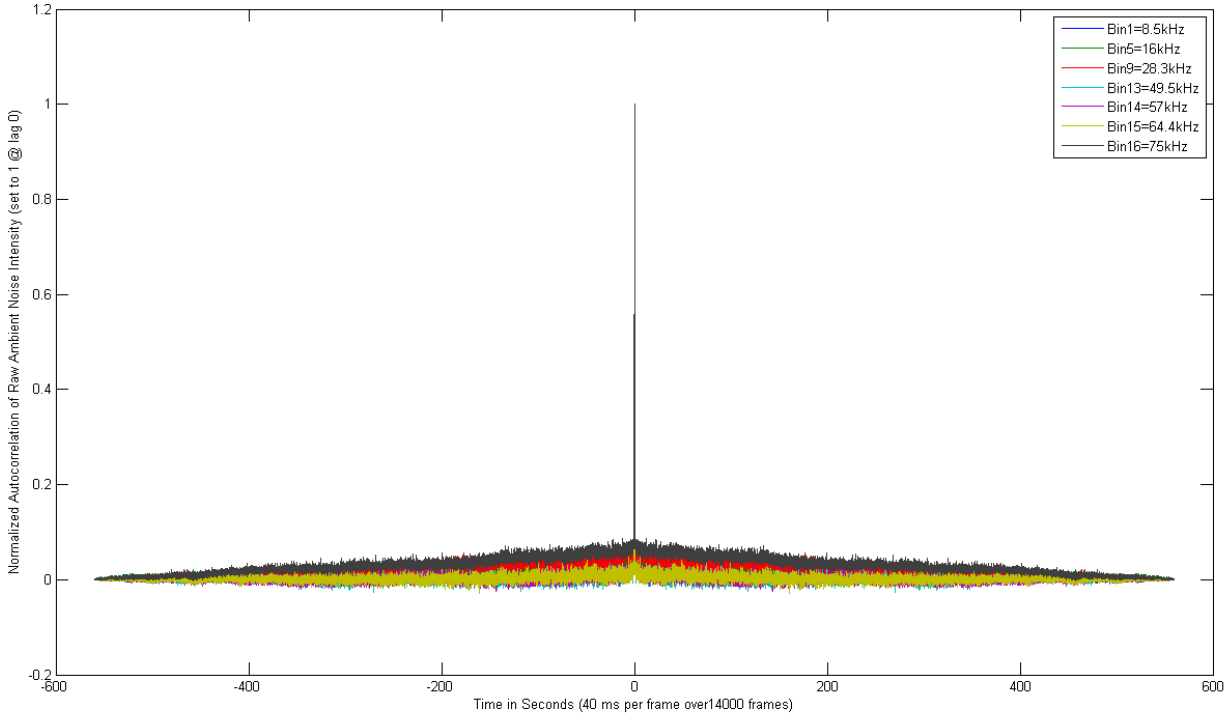

Figure 2.5: Normalized auto-correlations of the mean-biased initial 560 seconds of ambient noise intensity time series of data file number 15. The bias is applied by subtracting overall mean value (531.84 A/D counts) from each data point in each time series prior to auto-correlation. This figure is therefore the same as Figure 2.3 except for the mean-biased time-series input. Note the approximate delta-function shape of entire auto-correlation curve in the absence of any triangular windowing artifact. This curve closely resembles the zero-mean auto-correlation curves for white noise (red and black) presented in Figure 2.2.

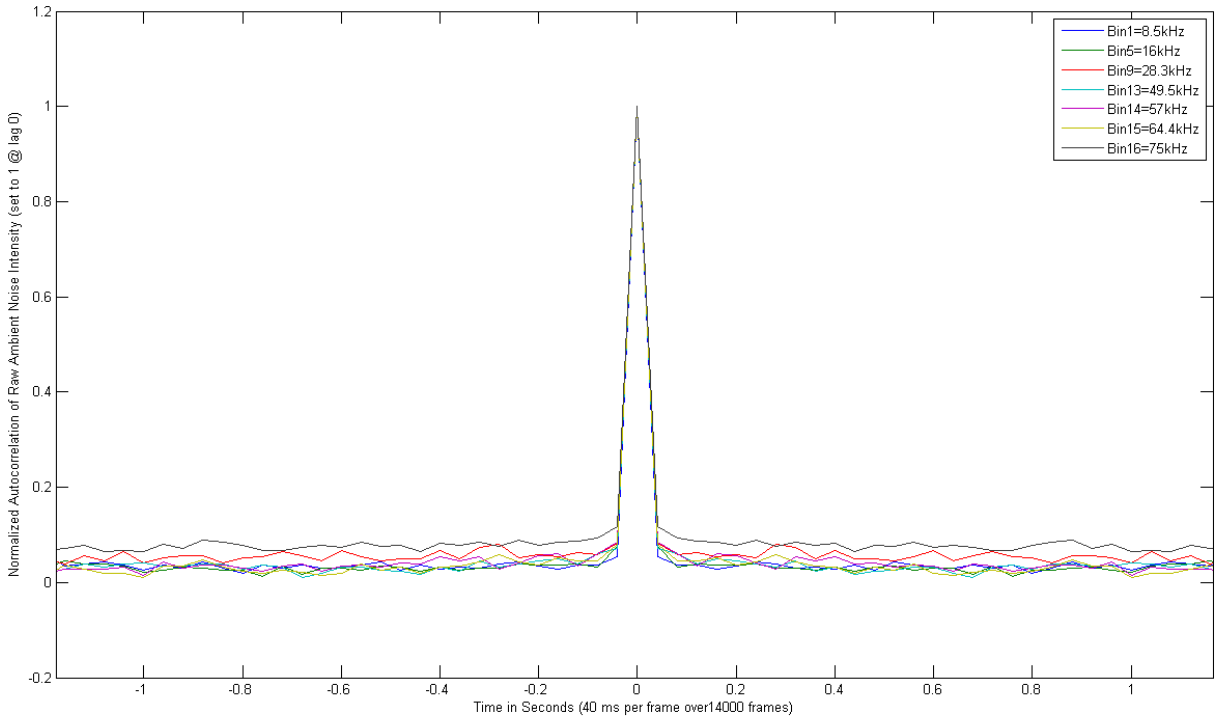

Figure 2.6: Horizontally-constrained zoom of Figure 2.5 illustrating the behaviour of the auto-correlation curve near $t = 0$. Note the trivially rapid de-correlation of the ambient noise intensity over the a 0.04 second (or one frame) time lag. The auto-correlation of the ambient noise intensity in a static-configuration segment of data file number 15 does indeed very closely approximate the delta function, the auto-correlation of white noise.

Chapter 3

Acoustic Daylight Image Target Recognition

The primary method of object recognition described in this chapter is based on the mathematics of principal component analysis, or PCA. PCA makes use of the eigenvalue decomposition of a covariance matrix as a means to differentiate one object from others based on its features, or principal components [Jolliffe, 2002]. This chapter describes the implementation of the PCA-based object recognition procedure, as well as the results of various recognition experiments performed using both original and modified ADONIS images as query and database image sets.

3.1 PCA Algorithm for ADONIS Images

A database of known acoustic daylight images is developed, consisting of matrix representations of ADONIS image data in MATLAB (.mat) format. The image data is extracted from the original data files, equalized from linearized ambient data and calibrated in the usual way. Each individual database image represents a temporal average of several dozen (usually 250) consecutive good frames to ensure image stability given the temporally variable ambient noise field. Each image is packaged into a 11-by-14 matrix, the spatial configuration of which is consistent with the configuration of the ADONIS hydrophone array. In other words, each pixel in the matrix corresponds either to a pixel in either the elliptical ADO-

NIS array (where image information exists) or the non-array background (where no image information exists). The values in each pixel correspond to the acoustic daylight image intensity. Non-interpolated visual renderings (in .jpg format) with identical filenames are included in the database folder to assist in manual identification of the array representations. The database is meant to contain distinct ADONIS images of known objects that will matched to ADONIS images query of unknown objects, using the recognition algorithm.

A query image in MATLAB (.mat) format, packaged into the same 11-by-14 matrix representation of the elliptical ADONIS array, is chosen for the recognition procedure. An ideal image is one with visually similar characteristics to one of the database images. Where possible, the query image should be created by averaging a sequence of frames representing an object that is relatively clearly defined, and has a possible injective relationship with one of the database objects. All database images and query images must be represented in the same standard format. Specifically, the elliptical array within the 11-by-14 matrix with a uniform, non-data (uniform) background outside the ellipse, and the values inside the ellipse increase in value as the intensity of the acoustic daylight signal increases. Inside the ellipse, the higher values represent the presence of a target object and lower intensity values represent the lack of a target object in the surrounding water).

First, the set of deviations from the mean images is constructed in the following manner. The database image matrices (.mat files) are loaded into the MATLAB workspace. The set of database image matrices is denoted: $X = [X_1; X_2; ...; X_n]$, where n is the number database images. The overall maximum intensity value (over all image intensity values), I_{max} is obtained and all image intensity values are normalized within the range $[0, 1]$. A mean normalized database image, X_{avg}, is created by averaging all normalized database images into a single 11-by-14 matrix. The maximum intensity in X_{avg} is $I_{max}/I_{max} = 1$. A set of images Y representing deviations from the mean is created by subtracting X_{avg} from each image X_i in X, so that $Y = [Y_1; Y_2; ...; Y_n] = [X_1 - X_{avg}; X_2 - X_{avg}; ...; X_n - X_{avg}]$.

Second, each image in the database is projected onto the database's universal eigenspace [Jolliffe, 2002]. The method is as follows. A positive definite square

matrix representing the covariance $Z = YY^T$ is constructed. Z has eigenvalues λ_i (a chosen finite set of which is $[\lambda_1, \lambda_2, ..., \lambda_k]$) and corresponding eigenvectors e_i (a chosen finite set of which is $[e_1; e_2; ...; e_k]$). The set of eigenvectors e_i (or, 'eigenimages') define the database's universal eigenspace, $E = [e_1; e_2; ...; e_k]$. Each database image is then projected onto the universal eigenspace E. The set of images projected onto the universal eigenspace is represented by $G = [g_1, g_2, ..., g_n]$, and the k-tuple for each projection of X_i onto E is: $g_i = E^T Y_i = [e_1; e_2; ...; e_k]^T [X_i - X_{avg}]$. The eigenvalues and eigenvectors are then sorted in order of decreasing eigenvalue, ensuring that the pairings between eigenvalue and eigenvector are maintained. The value k is the number of eigenvalues computed (equal to the number of eigenvectors computed), where λ_1 is the (overall) largest eigenvalue and λ_k is the smallest out of the finite set of eigenvalues computed (not necessarily the smallest overall eigenvalue). The value of k can vary, but should be large enough so that the most significant image features are accounted for, though not so large that too many insignificant features skew the result.

Third, the recognition procedure is carried out for a chosen query image. The query image is extracted, equalized, calibrated and packaged in the same way as the database images, yielding an 11-by-14 matrix Q. Q is normalized in the same manner as the database images. The deviation from the mean $R = [Q - X_{avg}]$ is calculated and R is projected onto the universal eigenspace E in the same manner as the database images to yield $F = [f_1, f_2, ..., f_n]$. G and F can be considered vectors in Euclidean n-space. The recognition procedure identifies the best match between the query image and the database images by finding the $[f, g]$ pair with the smallest Euclidean distance d between them in k-space (where k is less than or equal to n): $d = ((g_1 - f_1)^2, (g_2 - f_2)^2, ..., (g_k - f_k)^2)^{1/2}$. The number of $[f, g]$ pairs is equal to k, the number of eigenvalue-eigenvector pairs calculated earlier. The quality of the matches is in the reverse order of the Euclidean distance between the set of $[f, g]$ pairs. The query image and the top database image matches can then be visually presented by displaying the top images in order of their corresponding values of d.

3.2 Recognition Experiments

A short experiment using the PCA algorithm performed on a subset five ADONIS acoustic daylight images. Each image features a distinct type of target object: the planar holey cross, a planar bar, the three suspended drums, a bottom drum, and a sphere. The original versions of these images are shown in Figure 3.1 in both their non-interpolated and interpolated forms. Recognition experiments are performed on original non-interpolated image data and the interpolated images are for post-processing enhancement only. The output format, unless otherwise specified, consists of two rows of images, non-interpolated images in the top row and their interpolated counterparts in the bottom row. The first column represents the query image, and the rest of the columns (the number varies, but there are typically three or four) are the best database image matches, in order of increasing Euclidean distance. The database consists the five ADONIS images described above, generally manipulated or differing in some way from the original images. The number of top eigenvalues computed, k, may varied and can significantly affect the computed Euclidean distance values; it can therefore significantly affect the outcome of the experiment.

In an initial trivial experiment, the query image is the holey cross image and the database consists of the aforementioned eleven images including the holey cross. Predictably, the recognition algorithm selects the holey cross image as the best match, with a Euclidean distance of zero. The number, k, of eigenvalues computed in this trivial example is unimportant (as far as the top result is concerned), since when given an query image that also exists in the database, the algorithm will select that same image as the top match with a Euclidean distance of zero, given any arbitrary integer k value greater than zero. In this case, k was set to one.

The next set of experiments involves various transformations of the five images shown in Figure 3.1. The database consists of three sets of these five images, hereafter referred to as the "original set." In the first experiment, the effectiveness of the database on flipped images is examined. The first set is the same as the original set, with the data averaged over the top three frequency bins as before, except the data has been flipped left-to-right, that is, the leftmost

column's pixels are swapped with the rightmost column's pixels while maintaining row order, and so forth. The second set is again the same as the original set except the data base been flipped top-to-bottom. The third set is the original set flipped both left-to-right and then top-to-bottom. The query images are from the original set, and k is set to ten. The results are presented in Figures 3.2 and 3.3. The results generated for both bottom air drum and holey cross query images typify results for the other three query images as well as for values of k beyond one (with some minor variation in the ordering of second through fourth best results), so the discussion here applies in general to the original set images when used as queries to the flipped image database.

The results in Figure 3.2 demonstrate that the PCA recognition algorithm performs reasonably well for ADONIS images like that of the bottom air drum after various reflection mappings (flips) about perpendicular central axes. Indeed, all three different flipped database versions of the bottom air drum feature in the top four results (with k-space Euclidean distances of about 2.81, 4.47 and 5.28, respectively), with only the third result giving a different object (the planar metal bar, with a Euclidean distance of about 4.51). The prominent features of the bottom air drum image include a centrally located horizontal 'band' of high intensity with two prominent adjacent 'dots' of highest intensity within the greater 'band.' Also prominent are the medium intensity 'halo' regions above and below the high intensity band which slowly degrade toward the outer boundaries of the elliptical data region. All four bottom air drum images exhibit these features. The difference between the air drum image that comes up at the fourth-best match (twice flipped: left-right and up-down) and the first two seems to be the homogeneous areas of medium to medium-high intensity both below and to the right of the target in the twice flipped image, while the query image and the top two matches (once flipped air drums) have the medium to medium-high intensity regions either above or to the left of the target. The only non-air drum match, the metal bar, has the medium-intensity regions above the target but not to the right. The metal bar image also has a high-intensity target area in the same and of nearly the same size as the high-intensity target area in the air drum images. It is likely for this reason

that the metal bar is picked above the twice-flipped air drum image. A potential solution to this problem might be to conduct some pre-processing in the form of a threshold to keep the high-intensity target area and eliminate the medium intensity 'halo' areas. This would essentially leave only the high-intensity targets, which, under a future recognition experiment, yield all three air drum images as the top three matches since the targets would all me more alike and in similar locations while the metal bar image would have its target in a similar central location but would be less alike since the target would have more of circular or square shape rather than the centrally-located horizontal band shape of the air drum images.

The results in Figure 3.3 illustrate some of the major weaknesses of the PCA recognition algorithm when applied to ADONIS images. While the algorithm does pick one of the flipped holey cross images (the up-down flip), it then goes on to pick various images of other targets as the the next three top matches. In fact, the other two holey cross images (left-right and twice flipped) are not picked until the end of the match order (fourteenth and fifteenth out of fifteen). The reason for this is most likely due to the location of the highest intensity feature in the image: the left panel of the cross. The 'dot' representing its intensity peak is about fifteen to thirty percent higher than the intensity of the other three holey cross panels, even through all four panels have a much higher intensity than the rest of the image. This type of high-intensity 'dot' is found in all of the normalized database images. As a result of the normalization, any high-intensity 'dot' present in the middle-left of the elliptical data region will closely resemble the high-intensity 'dot' of the left holey cross panel, evident in the query image and the first match, and will end up curbing the k-space Euclidean distance heuristic dramatically. Indeed, it turns out that all flipped versions of the four non-holey cross images, after normalization, have such similar high-intensity 'dot' features nearer to the location of the left holey cross panel in the query image (centre or centre-left) than do the left-right flipped holey cross images which end up having a dot to the far left-centre of the elliptical data area. This centre-to-centre-left highest-intensity dot trumps the Euclidean distance metric despite the presence of the three slightly-less high-intensity dot pattern of the holey cross in the two left-right flipped images, which

make these images (to the human eye) more similar to the query image than any of the other non-holey cross database images. A potential remedy to this problem would be to perform pre-processing in the form of an intensity equalization akin to a basic intensity histogram equalization transformation. This would help make all four high-intensity 'dot' features representing the holey cross panels of approximately equal intensity. This would give each of them approximately equal weight as prominent features in the eigenvalue representation and therefore also in the Euclidean distance heuristic calculation. Other modifications such as thresholding and cropping (so that the target is more 'centred' in the elliptical data area) would most likely also contribute to more accurate matching in future experiments.

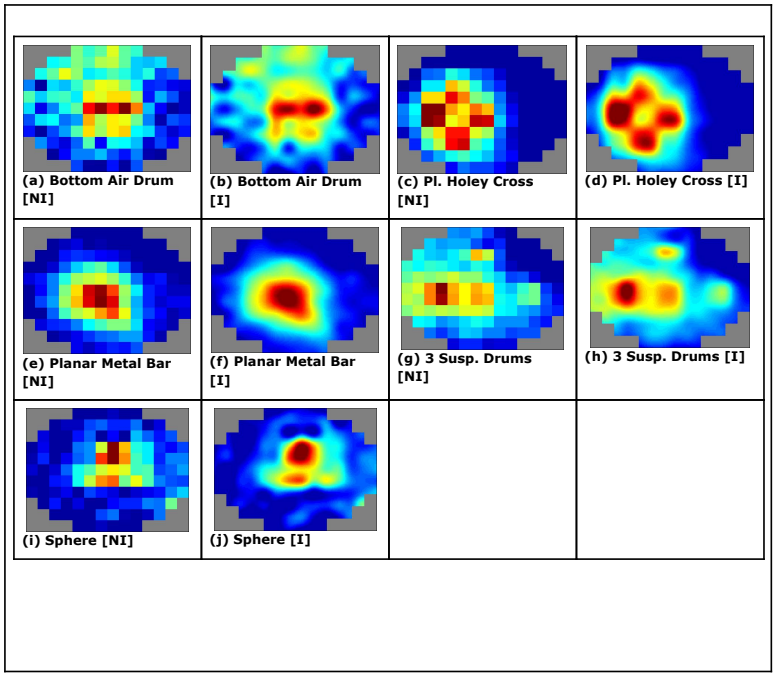

Figure 3.1: The five images used in the initial recognition experiments; non-interpolated [NI] and interpolated [I] forms.

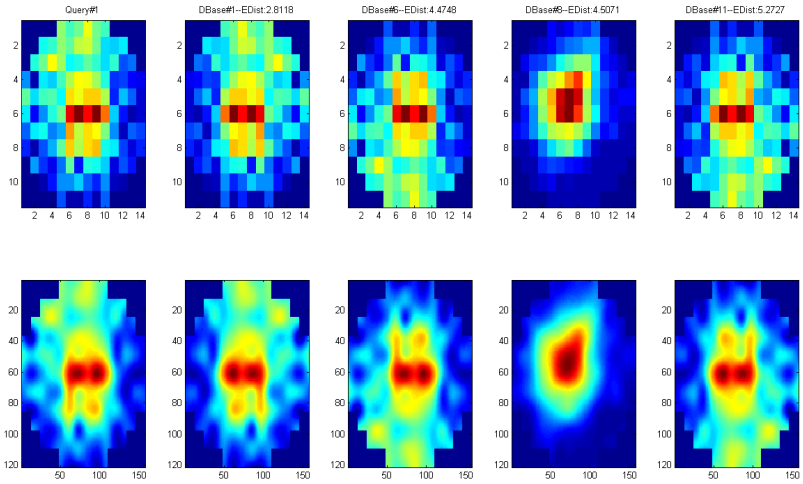

Figure 3.2: PCA recognition experiment results for a database containing flipped (left-right, up-down, and both) versions of the original 5 images. The query image is the bottom air drum.

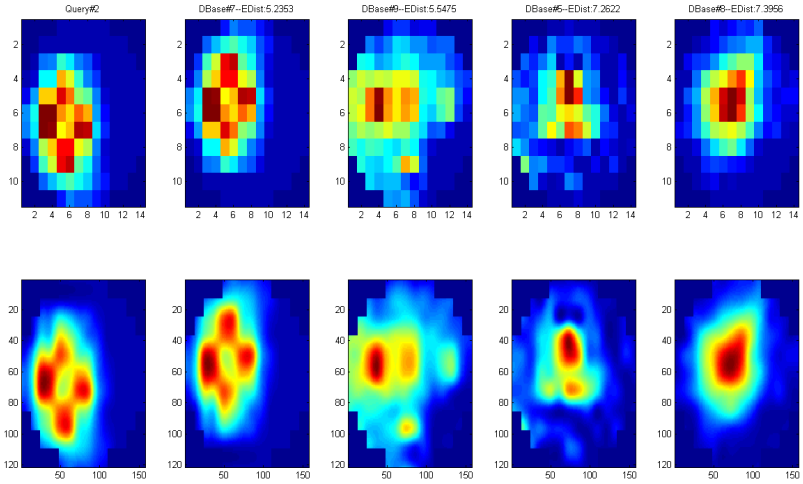

Figure 3.3: PCA recognition experiment results for a database containing flipped (left-right, up-down, and both) versions of the original 5 images. The query image is the holey cross.

Bibliography

[1] M.J. Buckingham. *Noise in Electronic Devices and Systems.* Ellis Horwood Limited, Chichester, West Sussex, England, 1983.

[2] C. L. Epifanio. *Acoustic Daylight: Passive Acoustic Imaging Using Ambient Noise.* PhD thesis, University of California, San Diego, San Diego, CA, 1997.

[3] Chad L. Epifanio, John R. Potter, Grant B. Deane, Mark L. Readhead, and Michael J. Buckingham. Imaging in the ocean with ambient noise: the orb experiments. *J. Acoust. Soc. Am.*, 106:3211–3225, 1999.

[4] I.T. Jolliffe. *Principal Component Analysis.* Springer, New York, 2nd edition, 2002.

[5] G. Marsaglia and W.W. Tsang. The ziggurat method for generating random variables. *Journal of Statistical Software*, 5(8), 2000.

[6] S.J. Orfanidis. *Optimum Signal Processing. An Introduction.* Prentice-Hall, Englewood Cliffs, NJ, 2nd edition, 1996.